HHS Public Access

Author manuscript

Cancer Lett. Author manuscript; available in PMC 2017 August 13.

Published in final edited form as:

Cancer Lett. 2016 May 28; 375(1): 62–72. doi:10.1016/j.canlet.2016.02.042.

Hexamethylene amiloride engages a novel reactive oxygen species-and lysosome-dependent programmed necrotic mechanism to selectively target breast cancer cells

Ashley R. Rowson-Hodel, **Anastasia L. Berg**, **Jessica H. Wald**, **Jason Hatakeyama**, **Kacey VanderVorst**, **Daniel A. Curiel**, **Leonardo J. Leon**[1], **Colleen Sweeney**, and **Kermit L. Carraway III**[*]

Department of Biochemistry and Molecular Medicine and University of California Davis Comprehensive Cancer Center, University of California Davis School of Medicine, Sacramento, CA, USA

Abstract

Anticancer chemotherapeutics often rely on induction of apoptosis in rapidly dividing cells. While these treatment strategies are generally effective in debulking the primary tumor, post-therapeutic recurrence and metastasis are pervasive concerns with potentially devastating consequences. We demonstrate that the amiloride derivative 5-(*N,N*-hexamethylene) amiloride (HMA) harbors cytotoxic properties particularly attractive for a novel class of therapeutic agent. HMA is potently and specifically cytotoxic toward breast cancer cells, with remarkable selectivity for transformed cells relative to non-transformed or primary cells. Nonetheless, HMA is similarly cytotoxic to breast cancer cells irrespective of their molecular profile, proliferative status, or species of origin, suggesting that it engages a cell death mechanism common to all breast tumor subtypes. We observed that HMA induces a novel form of caspase- and autophagy-independent programmed necrosis relying on the orchestration of mitochondrial and lysosomal pro-death mechanisms, where its cytotoxicity was attenuated with ROS-scavengers or lysosomal cathepsin inhibition. Overall, our findings suggest HMA may efficiently target the heterogeneous populations of cancer cells known to reside within a single breast tumor by induction of a ROS- and lysosome-mediated form of programmed necrosis.

Keywords

Breast cancer; Necrosis; Apoptosis; Cytotoxicity; Cancer therapeutics

Introduction

While the past several decades have witnessed unparalleled advances in our understanding of the cellular and molecular mechanisms regulating cancer initiation and progression,

[*]Corresponding author: Tel.: +1 916 734 3114; fax: 916 734 0190. klcarraway@ucdavis.edu (K.L. Carraway III).
[1]Current address: Skaggs School of Pharmacy and Pharmaceutical Sciences, UC San Diego, La Jolla, California, USA.

Conflict of interest

None.

substantial challenges remain with respect to cancer treatment efficacy. Significantly, commonly employed chemotherapeutics often fail to distinguish between tumor and normal tissue, inducing the indiscriminate death of rapidly dividing cells such as those of the digestive tract, bone marrow, mucous membranes and hair follicles [1]. In addition, cancer cells are particularly resistant to apoptotic death induced by conventional and targeted therapies [1], engaging pro-survival pathways such as phosphatidylinositol-3 kinase (PI3K)/Akt and extracellular regulated kinase (Erk; [2]) while inhibiting pro-apoptotic pathways [3]. Thus, agents that can distinguish normal from cancer cells, and that induce forms of cell death distinct from apoptosis and independent of cell cycling, may offer a superior therapeutic approach to improve patient outcomes.

The FDA-approved potassium-sparing diuretic amiloride was originally developed as a specific inhibitor of the epithelial sodium channel (ENaC) of renal collecting ducts [4]. When administered to cells at moderate (5–50 μM) to high (~0.5 mM) concentrations, amiloride can also inhibit sodium-hydrogen exchange (NHE; [5]), drug efflux channel activity [6] and urokinase receptor (uPAR) activity and expression [7–9], and perturb cellular metabolism via loss of ATP [10] and calcium and potassium transport [5]. Given these effects, it is not surprising that high concentrations of amiloride act in an anticancer capacity. Notably, amiloride reduced the growth of hepatoma, mammary adenocarcinoma and prostate tumor cells *in vivo*, inhibited the formation of mutagen-induced lesions in the liver, pancreas, and colon, and suppressed the establishment of meta-static lesions (reviewed in [11]). Collectively, these observations are consistent with the cytostatic and anti-migratory effects of amiloride when employed at concentrations known to inhibit NHE1 and other cell surface ion channels, as well as the extracellular protease urokinase plasminogen activator (uPA; [11]).

Interestingly, it has been reported that very high concentrations of amiloride (~0.5 mM) induce the death of glioma cells, and that this cytotoxicity cannot be mimicked by independently inhibiting NHE1 with cariporide [12]. Expanding on these observations, we and others have demonstrated that the amiloride derivative 5-benzylglicinal amiloride (UCD38B) is cytotoxic toward cultured glioma [12,13] and breast cancer cells [14]. In both cases, UCD38B cytotoxicity was attributed to the induction of a caspase-independent, non-apoptotic cell death resembling programmed necrosis [13,14]. Further investigation suggested that UCD38B-induced cytotoxicity toward glioma cells correlates with the mis-trafficking of components of the uPA system following drug treatment [15]. Taken together, these data point to UCD38B as a potential treatment for refractory cancers. However, the high dose of UCD38B (>100 μM) required to efficiently elicit specific anti-cancer effects precludes its clinical utility.

Our previous observations point to a strong correlation between the cytotoxicity of amiloride derivatives and their ability to access the cell interior [13,14], suggesting that cytotoxic amilorides may act on one or more intracellular targets to trigger programmed necrotic cell death. Our observations also suggest that modification of the amine at the C(5) carbon of amiloride with hydrophobic moieties (Fig. 1A) augments cytotoxic potency, likely by elevating cell permeability of the derivatives. Here we demonstrate that the highly hydrophobic analog 5-(*N,N*-hexamethylene) amiloride (HMA) acts at micromolar

concentrations to induce the programmed necrotic death of cultured breast cancer cells via a novel lysosome- and reactive oxygen species (ROS)-dependent mechanism. Critically, we observe that HMA rapidly and selectively kills breast tumor cells relative to non-transformed cells derived from a variety of tissue types, and does so in a manner independent of the cell cycle. Taken together, our observations underscore the potential of HMA as a novel anti-cancer therapeutic that can specifically attack poorly proliferative tumor cell subpopulations by inducing their programmed necrotic death.

Materials and methods

Preparation of chemicals

Chemicals were added at indicated final concentrations (Supplementary Table S1) to nearly confluent cells. Inhibitors were added 1 hr prior to stimulation of cells with death-inducing agents, with the exception of 3-methyl adenine and chloroquine, which were added 24 hrs prior to stimulation. Vehicle only negative controls were included with each experiment.

Cell culture

MDA-MB-231, MCF7, SKBR3, T47D and nMuMG cells were purchased from American Type Culture Collection (ATCC, Manassas, VA, USA) and maintained as recommended in the presence of 10% fetal bovine serum (FBS, HyClone, Thermo Fisher Scientific, Ward Hill, MA, USA) and antibiotics (penicillin/streptomycin; Gibco, Thermo). T47D cells were supplemented with the growth factors insulin (#I9278; Sigma Aldrich, St. Louis, MO, USA) and epidermal growth factor (#01-107, EMD Millipore). MCF10A (ATCC) and HMEC4 (gifted by K. Rao [16]) were maintained in mammary epithelial basal media (MEBM; #NC952377, Thermo) with growth factors and antibiotics. Met-1 (gifted by A.D. Borowsky) and NDL cells were maintained as previously described [17,18]. Cell lines were authenticated prior to use by short-tandem repeat profiling (Genetics Core Facility; University of Arizona, Tucson, AZ, USA) and were replaced with a cryopreserved stock every six passages. Cell line attributes are summarized in Supplementary Table S2.

Primary pig intestinal cells were maintained as described [19] (provided by L. Garas, UC Davis; obtained from AT Bilkslager; [19]). Primary mouse cells were harvested from 8 to 12 week old FvB/NJ mice (n = 3 or 4 [renal epithelium]) after routine euthanasia by CO_2 inhalation as established by the UC Davis Animal Care and Use Committee. Primary uterine and lung cells were isolated by incubation in Roswell Park Memorial Institute (RPMI)-1640 supplemented with 2 mg/mL collagenase IV (Worthington Biochemical Corporation; Lakewood, NJ, USA) and 10% FBS at 37 °C with light agitation on a rotisserie-style rotator until dissociated (up to 3 hrs). Primary mouse cardiac, skeletal and renal cells were isolated using 0.05% trypsin-EDTA for 30 min at 37 °C without agitation. Dissociated cells were passed over a 40 μm cell strainer to remove large debris and collagen strands, centrifuged at 400 × g and resuspended in complete media with 2% penicillin, streptomycin and gentamicin. Mouse primary cells were maintained in RPMI (lung, uterine) or Dulbecco's modified Eagle's medium (DMEM; cardiac, skeletal) plus insulin, transferrin and selenium solution (Gibco, Thermo), 10% FBS and antibiotics. All primary cells were used within three passages of harvest.

Western blotting

Western blotting was performed as described [14] and proteins blotted after transfer to polyvinylidene difluoride (<35 kDa) or nitrocellulose membrane. Band density was quantified using Image J software (NIH; http://rsb.info.nih.gov/ij/) and normalized to a loading control (tubulin, actin). See Supplementary Methods for antibody details.

Lysosomal analysis

MCF7 breast cancer cells were loaded with acridine orange (100 mg/mL) for 30 minutes following a 3 hr treatment with either 40 μM HMA or vehicle only control (DMSO). Cells were washed with phosphate buffered saline and imaged immediately in fluoromount-g (Southern Biotech, Birmingham, AL) by fluorescence microscopy. Acidic vesicles were identified by excitation at 541 nm and emission at 572 nm, while nucleic acids were visualized by excitation at 490 nm and emission at 530 nm.

Cell death analyses

Trypan blue exclusion assay—Following treatment with death inducing agents or vehicle control, breast cancer cells were trypsinized (0.05% trypsin-EDTA) to complete detachment (3–10 min) and quenched with 10% FBS in respective base media. Cells were pelleted at 1200 × g and resuspended in 0.1% trypan blue in phosphate buffered saline and counted by hemocytometer.

Acridine orange (AO)/ethidium bromide (EB) assay—MDA-MB-231 and MCF7 cells were treated at 80% confluence with either 40 μM HMA or vehicle control in standard media for the indicated times. Cells were subsequently treated with AO-EB solution, immediately imaged and categorized as early apoptotic, late apoptotic or necrotic based on morphology and color as described [20]. Cell counts were obtained from ten replicate fields and categories expressed as a percent of total. Images were quantified in ImageJ.

Propidium iodide/annexin-V assay—Met-1 and nMuMG cells were treated with vehicle control (DMSO), 40 μM HMA, or 50 μM cisplatin (Sigma) for 24 hrs. Cells were then stained with Annexin V-Alexa Fluor 647 (#A23204, Life Technologies) and propidium iodide (#P4170-10 mg, Sigma) in Annexin Binding Buffer (50 mM HEPES, 700 mM NaCl, 12.5 mM $CaCl_2$, pH 7.4) as described by the manufacturer. Cells were sorted using a Becton Dickinson FACSCanto flow cytometer and analyzed using FloJo (version 7.6) software.

Electron microscopy—MCF7 cells were plated on Permanox chambered slides (Lab-Tek, Electron Microscopy Sciences; Hatfield, PA, USA), treated at 80% confluence with 40 μM HMA or vehicle control and prepared for electron microscopy as described [14].

Cyclin D1 knockdown

MDA-MB-231 and MCF7 cells were treated with CCND1 targeting siRNA or non-targeting siRNA (15 nM, Dharmacon) essentially as described [14] using PepMute siRNA transfection reagent (SignaGen) in serum- and antibiotic-free media. To confirm reduced proliferation following cyclin D1 knockdown, cells were fixed with ice-cold methanol and acetone (1:1; 10 min) 48 hrs after transfection and the nuclei stained with 4′,6-diamidino-2-

phenylindole (DAPI) solution (500 ng/mL; Invitrogen). Cells were imaged by fluorescence microscopy (Olympus IX-81), and the percent mitotic cells (bright, doublet nuclei) obtained from 10 independent fields.

Statistical analysis

Values are expressed as averages ± the standard error of the mean (SEM) and were calculated from a minimum of three replicate experiments. Statistical significance was established using an independent two-sample t-test with p-values less than 0.05 considered statistically significant.

Results

Our previous studies indicate that very high concentrations of amiloride or UCD38B induce the rapid death of cultured human breast cancer cells [14]. To determine whether the more hydrophobic HMA might have increased efficiency, we first examined the impact of this derivative on a battery of human and mouse transformed and non-transformed mammary epithelial cell lines. In short exposure (24 hrs) dose–response experiments, we found that HMA is cytotoxic toward all breast cancer cell lines tested (Fig. 1B), irrespective of their molecular profile or species of origin (Supplementary Table S2). Strikingly, HMA is significantly more cytotoxic toward cell lines derived from human breast cancers (MDA-MB-231, MCF7, SKBR3, T47D) and mouse mammary cancers (Met-1, NDL) than non-transformed human breast cells (HMEC4, MCF10A) or mouse mammary cells (nMuMG; Fig. 1B). Moreover, HMA is poorly toxic toward non-transformed mouse primary cells, including those isolated from the uterus, lung, kidney, skeletal muscle and heart (Fig. 1C). The differences in cytotoxicity between transformed and non-transformed cells could not be explained by variations in drug uptake because HMA, visible under UV-excitation conditions [21], concentrates intracellularly with equal efficiency in human breast cancer cells, mouse mammary cancer cells and non-transformed cells (Supplementary Fig. S1A). The selective targeting of tumor cells by HMA suggests that a pathway or process unique to cellular transformation may underlie HMA cytotoxic potency, and underscores the potential of this agent as an anti-cancer drug. Notably, the HMA cytotoxicity curves (Fig. 1B) are steeper than expected for a single drug acting toward a single target, indicative of a cooperative or complex mechanism.

In a direct comparison, we found that HMA is considerably more cytotoxic toward breast cancer cells than its parent compound amiloride. Specifically, 2- to 3-fold less HMA is required to effectively deplete half (EC50) of MCF7 and MDA-MB-231 cell populations (Supplementary Fig. S1B and C). The increased potency of HMA is most evident at the single 24 hr dose required to diminish 90% of breast cancer cell populations (EC90), where 7- to 11-fold less HMA is required to elicit the bulk depletion of MCF7 and MDA-MB-231 cells (Fig. 1B and Supplementary Fig. S1C). Importantly, we found the EC50 of HMA is dramatically reduced when administered as three repeated daily doses (72 hrs total) rather than as a single 24 hr dose (Supplementary Fig. S1D; MCF7, 8 μM versus 39.1 μM and MDA-MB-231, 13 μM versus 35.4 μM). However, all of our subsequent viability studies

described below utilize HMA at single 24 hr doses consistent with our established mean EC50 (40 μM) and EC90 (80 μM).

As conventional anti-cancer therapeutics primarily target actively dividing cells, a subset of dormant cells may remain post-treatment capable of reestablishing primary breast tumors or seeding metastatic lesions. To determine whether the cytotoxic effects of HMA are cell cycle-dependent, we examined the effect of cyclin D1 knockdown by siRNA on HMA-induced cell death in MCF7 and MDA-MB-231 cells. Knockdown efficiently suppresses cyclin D1 protein levels (Fig. 1D; MDA-MB-231 85.1 ± 8.5% 48 hrs and 96.2 ± 1.2% 72 hrs after transfection; MCF7 52.6 ± 4.4% 48 hrs and 28.9 ± 7.3% 72 hrs after transfection) and reduces proliferation 4- to 6-fold (Fig. 1E). However, inhibition of cell cycle progression does not affect the ability of HMA to induce death in breast cancer cells, reflected in a similar fold reduction in cell viability with HMA treatment after cyclin D1 knockdown as compared with scramble control (Fig. 1F; MCF7, 2.5 ± 0.4 fold reduction in scramble control versus 2.4 ± 0.3 with cyclin D1 knockdown, $p = 0.8$; MDA-MB-231, 4.9 ± 0.8 versus 6.3 ± 2.4 fold reduction; $p = 0.6$). Likewise, HMA depletes human breast cancer cells (Supplementary Fig. S2A; MCF7, $p < 0.001$; MDA-MB-231, $p < 0.01$) and mouse mammary cancer cells (Supplementary Fig. S2A; Met-1, $p < 0.05$) under serum starve conditions despite significant reductions in mitotic figures (Supplementary Fig. S2B; MCF7 $p < 0.05$; MDA-MB-231 $p < 0.01$; Met-1 $p < 0.05$). Taken together, these data indicate that active proliferation is not prerequisite for HMA-mediated cytotoxicity.

Our previous investigations indicated that UCD38B induces a form of cell death that is partially dependent on apoptosis-inducing factor (AIF) and its translocation from the mitochondria to the nucleus [13,14]. However, we have found no evidence for AIF involvement in HMA-induced cytotoxicity (not shown), suggesting that HMA may employ a distinct cellular mechanism. Cells undergoing canonical apoptosis are identifiable by the activation of caspases and nuclear condensation, whereas cells undergoing programmed necrosis display a characteristic swelling of intracellular organelles with the ultimate rupture of nuclei, mitochondria and the plasma membrane [22]. Consistent with a necrotic mechanism, we found that HMA does not promote the activation of caspase-7 (Supplementary Fig. S3A). Likewise, co-incubation with the pancaspase inhibitor zVADfmk does not significantly attenuate the cytotoxicity of HMA in any breast cancer (MCF7, MDA-MB-231, T47D, SKBR3) or mammary cancer (Met-1, NDL) cell line evaluated under conditions that impede apoptosis induced by the conventional chemotherapeutic agents docetaxel, doxorubicin and cisplatin (Fig. 2A).

To further clarify the mode of cell death and establish a time course for HMA-induced cytotoxicity, we utilized the vital fluorescent stains acridine orange (AO) and ethidium bromide (EB). Sequential AO and EB staining allows for the discrimination of early apoptotic, late apoptotic and necrotic cells on the basis of nuclear morphology and loss of plasma membrane integrity [23]. MCF7 (Fig. 2B and Supplementary Fig. S3B) and MDA-MB-231 (not shown) cells exposed to 40 μM HMA exhibit marked loss of membrane integrity without nuclear condensation, as revealed by EB and AO staining, respectively. The induction of necrosis is rapid, with uptake of EB within 2 hrs of exposure to HMA as compared to vehicle control ($p < 0.0001$). Rupture of the plasma membrane was confirmed

by the lactate dehydrogenase (LDH) release assay, a measurement of the extrusion of cytosolic contents from necrotic cells. Consistent with the AO-EB assay, we found LDH levels are significantly increased after 2 hrs of HMA exposure as compared to control (Supplementary Fig. S3C, $p < 0.05$).

Next, we evaluated the loss of cell membrane integrity by incorporation of propidium iodide and exposure of inner leaflet-associated phosphatidylserine. In apoptotic cells, phosphatidylserine externalization typically precedes PI positivity whereas in necrotic cells the two events are often coordinated [24]. Using Annexin-V to detect phosphatidylserine in combination with PI, we determined by FACS analysis that HMA induced significant cytotoxicity in Met-1 mammary cancer cells (Fig. 2D and Supplementary Fig. S3D), as indicated by a higher percentage of cells that were considered dead (PI positive, Annexin-V positive or dual positive 55.8 ± 9.4%) compared to vehicle only control (15 ± 3.2%; $p < 0.05$). Moreover, we found this effect to be cancer cell specific, reflected by the failure of HMA to induce death in non-transformed mouse mammary cells (Fig. 2C and Supplementary Fig. S3D; NMuMG 13.2 ± 0.1% cytotoxicity with HMA vs. 9.2 ± 1.5% vehicle only control). These data provide substantial support to our previous conclusions from the trypan blue exclusion assays (Fig. 1B and C).

We noted a significant increase in the proportion of Met-1 mammary cancer cells that were simultaneously positive for PI and Annexin-V when compared to those that were singly positive for Annexin-V (Fig. 2D and Supplementary Fig. S3D; 46.5 ± 5.6% versus 8.4 ± 3.4%; $p < 0.01$), suggesting a propensity toward necrosis (dual positive) over apoptosis (Annexin V only). This contrasted with Met-1 cells exposed to the apoptosis-inducing agent cisplatin, which elicited a more equal distribution of Annexin-V only and dual positive cells (Fig. 2D and Supplementary Fig. S3D). Although PI-Annexin-V staining does not permit the discrimination between primary necrosis and apoptosis with secondary necrosis [24], our observation that HMA cytotoxicity is caspase independent (Fig. 2A and Supplementary Fig. S3A) strongly suggests that HMA stimulates primary necrosis.

To firmly establish that HMA induces a necrotic-type death, we evaluated HMA treated breast cancer cells by electron microscopy. Indeed, MCF7 breast cancer cells exposed to either 40 μM or 80 μM HMA for 3 hrs exhibit features typical of necrosis, including maintenance of nuclear structure with oncosis, perinuclear accumulation of intracellular organelles, and a loss of plasma membrane integrity (Fig. 3A and B). In particular, HMA induces mitochondrial swelling (Fig. 3B, 40 μM HMA and 80 μM HMA, a). These observations were confirmed using the mitochondrial specific probe Mitotracker Red (Supplementary Fig. S3E). A 3 hr HMA exposure induces a marked loss in both the integrity and distribution of mitochondria, reflected in their fragmentation and perinuclear accumulation. Electron microscopic analysis also revealed that 80 μM HMA induces the appearance of multilamellar bodies (Fig. 3B, 80 μM, b), lysosomal organelles containing multiple concentric membrane layers that are often associated with increased lysosomal degradation [25].

To date, several forms of programmed necrosis have been described, including poly (ADP-ribose) polymerase (PARP)-dependent parthanatos and receptor-interacting kinase

(RIPK)-1- and -3-dependent necroptosis (reviewed in [26]). We found that HMA does not induce cleavage of PARP in breast cancer cells (Fig. 4A). Moreover, HMA-mediated cytotoxicity is unimpeded in breast cancer cells treated with the RIPK1 inhibitor necrostatin-1 [27] or the RIPK3 inhibitor dabrafenib [28] either independently (not shown) or in combination in MCF7 cells (43 ± 6% viability with HMA vs. 30.8 ± 3.2% HMA plus dabrafenib (Dfb) and necrostatin-1 (Nec-1; $p = 0.28$)), MDA-MB-231 cells (49.2 ± 2.2% vs. 54.7 ± 6%; $p = 0.5$), and Met-1 cells (42.4 ± 3.4% vs. 28.0 ± 7.2%; $p = 0.26$), under conditions where these agents inhibit necroptotic cell death induced by shikonin (Fig. 4B). Consistent with these data, we found that HMA does not induce the activation of MLKL (Fig. 4C and D), a RIPK3-dependent substrate [29,30].

Independent of parthanatos and necroptosis, necrosis may follow a rise in cytosolic calcium, elevated ROS, and/or intracellular acidification by lysosomes [31]. As such, we evaluated the viability of MCF7, MDA-MB-231 and Met-1 breast tumor cells exposed to HMA for 24 hrs following pretreatment with a calcium chelator (Bapta/AM), a ROS scavenger (N-Ac), or lysosomal protease inhibitors (calpain inhibitor VI and leupeptin). We found that the viability of cells pretreated with Bapta/AM is inconsistent across cell lines (Fig. 5A), significantly reduced in MCF7 (41.9 ± 3.3% viability with HMA vs. 13.5 ± 2.4% HMA plus Bapta/AM, $p < 0.05$), significantly improved in MDA-MB-231 (41.3 ± 2.1% vs. 67.6 ± 3.8%, $p < 0.05$), or trending toward improvement in Met-1 (44.0 ± 2.3% vs. 71.7 ± 9.7%, $p = 0.058$), under conditions where viability is rescued in ionomycin-treated cells (Supplementary Fig. S4A). Importantly, we found that the viability of HMA-treated cells was improved in all three cell lines after the reduction of ROS (Fig. 5A; MCF7 viability with HMA plus N-Ac 62.1 ± 0.8%, $p < 0.001$; MDA-MB-231 70.2 ± 5.3%, $p < 0.05$; Met-1 64.2 ± 6.6%, $p < 0.05$), in a manner similar to the rescue of cells after tert-Butyl hydrogen peroxide treatment (TBHP; Supplementary Fig. S4A).

Similarly, all breast cancer cell lines tested exhibit significant rescue of viability upon inhibition of calpains and lysosomal cathepsins with calpain inhibitor VI (Fig. 5B; MCF7 viability 85.8 ± 4.9%, $p < 0.00001$; MDA-MB-231 76.6 ± 5.4%, $p < 0.05$; T47D 81.9 ± 5.5%, $p < 0.01$; SKBR3 76.4 ± 9.4%, $p < 0.05$; Met-1 83.4 ± 12.3%, $p < 0.05$; NDL 79.2 ± 5.5% $p < 0.05$) or leupeptin (Supplementary Fig. S4B; MCF7 viability with HMA 41.4 ± 1.0% vs. HMA plus leupeptin 72.9 ± 1.1%, $p < 0.0001$; MDA-MB-231 45.3 ± 0.6% vs. 91.8 ± 2.5%, $p < 0.01$), indicating the cytotoxicity of HMA likely depends on a ROS- and lysosome-mediated form of necrosis.

We found that lysosomal protease inhibition or ROS scavenging significantly improved the viability of MDA-MB-231 breast cancer cells within 1 hr of HMA administration (Supplementary Fig. S4C, N-Ac $p < 0.05$; calpain inhibitor V $p < 0.0001$). An increase in ROS production with HMA treatment was confirmed by DCFH-DA assay, which revealed a significant and steady increase in ROS production between 2 and 4 hrs of exposure to 40 μM HMA in both MCF7 and MDA-MB-231 breast cancer cells (Supplementary Fig. S4D, $p < 0.05$), consistent with the period of N-Ac sensitivity (Supplementary Fig. S4C). These data highlight a role for ROS and lysosomal cathepsins as executioners of HMA-mediated cell death, and raise the possibility that cathepsin activation may precede increases in ROS.

The stress-activated MAP kinase Jnk may potentiate necrotic cell death by a number of mechanisms that lie both upstream and downstream of ROS [32,33]. Accordingly, we sought to determine whether HMA stimulates Jnk phosphorylation, and if so, whether this activation is dependent on ROS. We found that HMA induces the phosphorylation of Jnk in MDA-MB-231 cells without a change in total Jnk protein levels (Fig. 5C), while decreasing the phosphorylation of pro-survival proteins Akt and Erk (Fig. 5C). Importantly, we found that phosphorylated Jnk, Akt and Erk protein levels are restored with N-Ac treatment but not with Bapta/AM (Fig. 5C), suggesting a pro-death cascade initiated downstream of ROS. Moreover, we found that the phosphorylation of Jnk occurs coincident with the onset of necrosis, where there was a significant increase in phospho-Jnk protein levels after a 2 hr exposure to 40 μM HMA relative to vehicle only control (Fig. 5D and Supplementary Fig. S5A, $p < 0.05$). Nevertheless, the activation of Jnk appears to be dispensable for the cytotoxic effects of HMA. Breast cancer cells pretreated with the Jnk inhibitor SP600125 were depleted with HMA under conditions that effectively restored the viability of cells exposed to anisomycin, a potent activator of Jnk-mediated prodeath cascades (Fig. 5E and Supplementary Fig. S5B and C, MDA-MB-231 $p < 0.05$).

Given the potential role for lysosomes in HMA-mediated cell death and their vital contribution to autophagic processes we asked whether HMA induces autophagy, and if so, whether this response is essential to cell death. While autophagy is considered a cell survival strategy that preserves cell viability during stress, it may initiate cell death under conditions of sustained environmental insult [34]. Consistent with previous observations of amiloride derivative action in breast cancer cells [14] and colon cancer cells [35], we found that HMA upregulates the autophagy-related protein LC3-IIB (Fig. 6A), a lipid-modified product of LC3-1B. However, inhibition of autophagosome formation with 3-methyladenine (3-MA; [36]) was insufficient to attenuate HMA-mediated cytotoxicity (Fig. 6B; MCF7 $p = 0.16$, MDA-MB-231 $p = 0.51$, Met-1 $p = 0.42$) but was effective during serum starvation conditions (MCF7 $p < 0.001$, MDA-MB-231 $p < 0.05$, Met-1 $p < 0.05$), suggesting that HMA-treated cells are not depleted by sustained autophagy. Conversely, pretreatment of cells with the lysomotrophic agent chloroquine significantly reduced HMA-induced cytotoxicity (Fig. 6B; all $p < 0.05$). Although chloroquine blocks lysosomal acidification and autophagic degradation events, it is not a specific inhibitor of autophagy. Along these lines, staining of lysosomes with AO demonstrated a significant effect of HMA on the structure and distribution of lysosomes, where a notable increase in their aggregation and accumulation at perinuclear regions in MCF7 cells after 3 hr exposure to HMA was observed (Fig. 6C). Together, these observations point to an autophagy-independent role for lysosomes in HMA-induced cytotoxicity.

Mechanistic target of Rapamycin (mTOR) has recently been described as an essential component in the regulation of lysosomal distribution, biogenesis and activity [37] as well as a mediator of programmed necrosis [38]. Accordingly, we determined whether HMA-induced cytotoxicity could be modulated by inhibition of mTOR complex 1 (mTORC1). Treatment of MDA-MB-231 cells with HMA increases phosphorylation of the mTORC1 substrate S6 kinase between 2 and 6 hrs, with levels returning to near control after 24 hrs (Fig. 7A and B). Additionally, pretreatment with the mTORC1 inhibitor rapamycin significantly improves the viability of HMA-treated MCF7 (HMA 40.3 ± 3.1% viability vs.

HMA plus rapamycin 70.6 ± 1.1% viability; $p < 0.01$) and MDA-MB-231 (41.2 ± 2.7% vs. 77.3 ± 2.1%; $p < 0.001$) breast cancer cells (Fig. 7C). Co-incubation of N-Ac with rapamycin improved the viability of MCF7 breast cancer cells (89.3 ± 2.6%; $p < 0.001$) and MDA-MB-231 (81.7 ± 0.4%; $p < 0.01$) providing either significant benefit (MCF7, $p < 0.05$) or no additional benefit over rapamycin alone (MDA-MB-231; $p = 0.11$). Taken together, these data suggest that HMA mediated cytotoxicity depends on the activation of mTOR.

Discussion

Herein we demonstrate that the amiloride derivative HMA selectively depletes breast cancer cells relative to non-transformed cells by inducing their programmed necrotic death. The specific effects of HMA do not arise from the preferential accumulation of HMA within cancer cells; rather, transformed cells appear more sensitive to HMA engagement of programmed necrotic pathways than their non-transformed counterparts. Importantly, we found that HMA is cytotoxic to breast cancer cells regardless of their molecular profile or proliferative status. These findings hold significant clinical promise, as accumulating evidence supports the notion that breast cancer is a heterogeneous disease. Indeed, breast cancer encompasses not only a number of subtypes classified in terms of hormone receptor status, molecular profile, stage and grade, but also intra-tumor heterogeneity where genetically, phenotypically and behaviorally distinct subpopulations coexist within a given tumor and its metastases [39,40]. While breast cancers are often treated based on their predominant subtype, intra-tumor heterogeneity offers a particular challenge to complete tumor eradication, where tumor recurrence and subsequent metastasis are often attributed to resistant or dormant subpopulations of tumor cells that repopulate the tumor post therapy. As such, the clinical application of HMA or similar agents offers a compelling strategy to not only selectively affect primary tumor growth, but importantly, reduce subsequent recurrence and metastasis.

Previous studies have demonstrated the anti-proliferative, anti-tumorigenic and/or anti-metastatic properties of amiloride and some of its derivatives. While some have identified specific perturbations in cell cycle progression and DNA integrity [35], the majority of studies have focused on plasma membrane associated ion and proton transporters [11,12,41], and/or uPA as the therapeutic targets (reviewed in [11]). Along these lines, a recent study suggested that UCD38B-induced necrosis depends upon mis-trafficking of endocytosed uPAR [15]. Specifically, the aberrant perinuclear accumulation of uPAR containing endosomes in close proximity to mitochondria may induce mitochondrial membrane depolarization and release of the pro-death factor AIF [15]. While our data support mitochondrial dysfunction in mediating HMA associated cell death, evidenced by increased mitochondrial swelling, aggregation and ROS production, it is probable that endosomal trafficking may only be a consequence of amiloride derivative action and not required for cell death. It is likely that amiloride derivatives such as HMA directly interact with mitochondrial transporters or channels, a notion supported by previous work investigating the association of particular amiloride derivatives with intracellular organelles [42].

Coincident with mitochondrial perturbations and ROS production, we found that HMA suppresses the activation of the prosurvival kinases Akt and Erk. Both the PI3K-Akt/PKB

and Ras/Erk pathways are commonly elevated in cancer cells, often as a consequence of constitutive growth factor receptor signaling [43]. Interestingly, previous studies have demonstrated that amiloride antagonizes receptor tyrosine kinase function [44] and potentiates TRAIL-mediated apoptosis via Akt inactivation [45]. Taken together, these data support the notion that HMA could sensitize cancer cells to cell death programs by disrupting survival and growth strategies mediated by PI3K-Akt.

In addition to downregulating prosurvival pathways, we found that HMA treatment induced the kinase Jnk downstream of ROS. Several studies have linked Jnk with both death receptor-dependent [46,47] and -independent [48] necrosis following exogenous ROS administration. Interestingly, activation of Jnk augments sensitivity to stress stimuli in transformed cell lines and primary mouse tumors relative to non-transformed cells [49]. The activation of Jnk was directly linked to enhanced ROS levels unique to transformed cells [49], suggesting that at least some of the specificity of HMA for breast cancer cells may arise from an inherently lower threshold for ROS when compared to normal breast cells.

In addition to perturbations of mitochondria, we found that HMA disturbed lysosome function, promoting their aggregation and the accumulation of multilamellar bodies. Interestingly, multilamellar bodies are correlated with increased lysosomal degradation during autophagy and are inhibited by treatment with the lysosomal protease inhibitor leupeptin or the autophagosome inhibitor 3-methyladenine [25]. We observed significant HMA induction of the autophagic process as suggested by a specific increase in LC3-IIB, consistent with previous reports of UCD38B action in breast cancer cells [14] and HMA action in colon cancer cells [35]. While the inhibition of autophagy with 3-methyladenine failed to rescue HMA-treated breast cancer cells, the inhibition of lysosomal proteases using the lysomotrophic agent chloroquine or panlysosomal protease inhibitors calpain inhibitor VI and leupeptin significantly blunted HMA-induced cytotoxicity. These data strongly suggest that while HMA induces lysosomal alterations that accompany autophagy, independent lysosomal events drive HMA-mediated cytotoxicity.

In further support of HMA utilizing a lysosome-mediated mechanism to induce cell death in breast cancer cells, we found that inhibition of mTORC1 with rapamycin significantly attenuated HMA-induced cytotoxicity. Lysosomes and mTOR are intimately associated, where the levels of amino acids within the lumen of the lysosome dictate mTORC1 activity [50]. Paradoxically, despite Akt being a known activator of mTOR, we found that HMA treatment promoted an increase in the mTORC1 substrate phospho-S6 kinase and decrease in Akt. It is possible that mTOR is directly activated following HMA treatment due to its inhibition of lysosomal nutrient sensing. Recent evidence suggests that mTORC1 is modulated via fluctuations in amino acid levels sensed at the vacuolar H^+ adenosine triphosphatase (v-ATPase; [50]). As the v-ATPase is also essential for maintaining the low luminal pH found in lysosomes and our data suggest that HMA activates pH-sensitive lysosomal proteases such as cathepsin B, it is a particularly intriguing potential target. Furthermore, several studies have suggested that amiloride and some of its analogs inhibit plasma membrane associated ATPases [51], giving further credence to this postulate. Finally, cancer cells may be particularly sensitive to v-ATPase targeting because the clinically employed potassium-hydrogen exchange antagonist omeprazole also inhibits lysosomal v-

ATPase activity to induce a cathepsin- and caspase-mediated apoptosis in leukemia cells *in vitro* [52].

In conclusion, we demonstrate that HMA holds particular clinical promise, indiscriminately targeting breast cancer cells irrespective of their molecular type or proliferative status without acting on a broad range of normal, non-transformed cell populations. It is likely that the specificity of HMA for cancer cell killing hinges upon several factors, including the induction of ROS, the downregulation of prosurvival pathways (Akt, Erk) and the release or activation of lysosomal proteases. Together, these events culminate in the induction of a form of programmed necrosis independent of the commonly cited RIPK-dependent necroptosis or PARP-dependent parthanatos. Our observations suggest that HMA interacts with intracellular targets to induce cell death, likely perturbing proton and ion gradients at key organelles such as mitochondria and lysosomes.

Supplementary Material

Refer to Web version on PubMed Central for supplementary material.

Acknowledgments

We thank L. Garas for kindly providing primary porcine intestinal cells, and M. Umeh-Garcia, J. Van Dyke (Technical Director, UC Davis Cell Sorting Core Facility), P. Kysar and staff (UC Davis Electron Microscopy Core Facility) for technical assistance. We gratefully acknowledge the support of the UC Davis Comprehensive Cancer Center Support Grant P30CA093373 and T32 training fellowship CA108459 (A. R. Rowson-Hodel).

Abbreviations

HMA	5-(*N,N*-hexamethylene) amiloride
DCFH-DA	carboxy-2′,7′-dichloro-dihydro-fluorescein diacetate
ROS	reactive oxygen species
PI3K	phosphatidylinositol-3 kinase
PKB	protein kinase B
Erk	extracellular regulated kinase
ENaC	epithelial sodium channel
NHE	sodium hydrogen exchanger
uPAR	urokinase receptor
UCD 38B	5-benzylglicinal amiloride
NAc	N-acetyl cysteine
TBHP	tert-Butyl hydrogen peroxide
zVADfmk	carbobenzoxy-valyl-alanyl-aspartyl-[O-methyl]-fluoromethylketone

DMSO	dimethyl sulfoxide
DMEM	Dulbecco's modified Eagle's medium
RPMI	Roswell Park Memorial Institute medium
EGF	epidermal growth factor
MEBM	mammary epithelial basal media
FBS	fetal bovine serum
LDH	lactate dehydrogenase
DAPI	4′,6-diamidino-2-phenylindole
RIPK	receptor-interacting kinase
LC3	light chain 3
MLKL	mixed lineage kinase domain like
AIF	apoptosis-inducing factor
PARP	poly (ADP-ribose) polymerase
PI	propidium iodide
mTOR	mechanistic target of rapamycin
mTORC1	mTOR complex 1
v-ATPase	vacuolar H^+ adenosine triphosphatase

References

1. Masui K, Gini B, Wykosky J, Zanca C, Mischel PS, Furnari FB, et al. A tale of two approaches: complementary mechanisms of cytotoxic and targeted therapy resistance may inform next-generation cancer treatments. Carcinogenesis. 2013; 34:725–738. [PubMed: 23455378]
2. Liu SQ, Yu JP, Yu HG, Lv P, Chen HL. Activation of Akt and ERK signalling pathways induced by etoposide confer chemoresistance in gastric cancer cells. Dig Liver Dis. 2005; 38:310–318.
3. Marquez RT, Tsao BW, Faust NF, Xu L. Drug Resistance and Molecular Cancer Therapy: Apoptosis Versus Autophagy. 2013
4. Salako LA, Smith AJ. Changes in sodium pool and kinetics of sodium transport in frog skin produced by amiloride. Br J Pharmacol. 1970; 39:99–109. [PubMed: 5420148]
5. Kleyman TR, Cragoe EJ Jr. Cation transport probes: the amiloride series. Methods Enzymol. 1990; 191:739–755. [PubMed: 1963659]
6. Ponte-Sucre A. Availability and applications of ATP-binding cassette (ABC) transporter blockers. Appl Microbiol Biotechnol. 2007; 76:279–286. [PubMed: 17522856]
7. Vassalli JD, Belin D. Amiloride selectively inhibits the urokinase-type plasminogen activator. FEBS Lett. 1987; 214:187–191. [PubMed: 3106085]
8. Wang Y, Jones CJ, Dang J, Liang X, Olsen JE, Doe WF. Human urokinase receptor expression is inhibited by amiloride and induced by tumor necrosis factor and phorbol ester in colon cancer cells. FEBS Lett. 1994; 353:138–142. [PubMed: 7926038]

9. Wang Y, Dang J, Liang X, Doe W. Amiloride modulates urokinase gene expression at both transcription and post-transcription levels in human colon cancer cells. Clin Exp Metastasis. 1995; 13:196–202. [PubMed: 7750207]
10. Lubin M, Cahn F, Coutermarsh BA. Amiloride, protein synthesis, and activation of quiescent cells. J Cell Physiol. 1982; 113:247–251. [PubMed: 6294122]
11. Matthews H, Ranson M, Kelso MJ. Anti-tumour/metastasis effects of the potassium-sparing diuretic amiloride: an orally active anti-cancer drug waiting for its call-of-duty? Int J Cancer. 2011; 129:2051–2061. [PubMed: 21544803]
12. Hegde M, Roscoe J, Cala P, Gorin F. Amiloride kills malignant glioma cells independent of its inhibition of the sodium-hydrogen exchanger. J Pharmacol Exp Ther. 2004; 310:67–74. [PubMed: 15010500]
13. Pasupuleti N, Leon L, Carraway KL, Gorin F. 5-Benzylglycinyl-amiloride kills proliferating and nonproliferating malignant glioma cells through caspase-independent necroptosis mediated by apoptosis-inducing factor. J Pharmacol Exp Ther. 2013; 344:600–615. [PubMed: 23241369]
14. Leon LJ, Pasupuleti N, Gorin F, Carraway KL III. A cell-permeant amiloride derivative induces caspase-independent, AIF-mediated programmed necrotic death of breast cancer cells. PLoS ONE. 2013; 8:e63038. [PubMed: 23646172]
15. Pasupuleti N, Grodzki AC, Gorin F. Mis-trafficking of endosomal urokinase proteins triggers drug-induced glioma nonapoptotic cell death. Mol Pharmacol. 2015; 87:683–696. [PubMed: 25634671]
16. Cheng JM, Ding M, Aribi A, Shah P, Rao K. Loss of RAB25 expression in breast cancer. Int J Cancer. 2006; 118:2957–2964. [PubMed: 16395697]
17. Miller JK, Shattuck DL, Ingalla EQ, Yen L, Borowsky AD, Young LJT, et al. Suppression of the negative regulator LRIG1 contributes to ErbB2 overexpression in breast cancer. Cancer Res. 2008; 68:8286–8294. [PubMed: 18922900]
18. Borowsky AD, Namba R, Young LJ, Hunter KW, Hodgson JG, Tepper CG, et al. Syngeneic mouse mammary carcinoma cell lines: two closely related cell lines with divergent metastatic behavior. Clin Exp Metastasis. 2005; 22:47–59. [PubMed: 16132578]
19. Schierack P, Nordhoff M, Pollmann M, Weyrauch K, Amasheh S, Lodemann U, et al. Characterization of a porcine intestinal epithelial cell line for in vitro studies of microbial pathogenesis in swine. Histochem Cell Biol. 2006; 125:293–305. [PubMed: 16215741]
20. Kasibhatla S, Amarante-Mendes GP, Finucane D, Brunner T, Bossy-Wetzel E, Green DR. Acridine orange/ethidium bromide (AO/EB) staining to detect apoptosis. CSH Protoc. 2006; 2006 pdb.prot4493.
21. Giansanti V, Santamaria G, Torriglia A, Aredia F, Scovassi A, Bottiroli G, et al. Fluorescence properties of the Na+/H+ exchanger inhibitor HMA (5-(N,N-hexamethylene) amiloride) are modulated by intracellular pH. Eur J Histochem. 2012; 56:e3. [PubMed: 22472891]
22. Searle J, Kerr JF, Bishop CJ. Necrosis and apoptosis: distinct modes of cell death with fundamentally different significance. Pathol Annu. 1982; 17(Pt 2):229–259. [PubMed: 7182752]
23. Ribble D, Goldstein NB, Norris DA, Shellman YG. A simple technique for quantifying apoptosis in 96-well plates. BMC Biotechnol. 2005; 5:12. [PubMed: 15885144]
24. Vanden Berghe T, Grootjans S, Goossens V, Dondelinger Y, Krysko DV, Takahashi N, et al. Determination of apoptotic and necrotic cell death in vitro and in vivo. Methods. 2013; 61:117–129. [PubMed: 23473780]
25. Hariri M, Millane G, Guimond MP, Guay G, Dennis JW, Nabi IR. Biogenesis of multilamellar bodies via autophagy. Mol Biol Cell. 2000; 11:255–268. [PubMed: 10637306]
26. Berghe TV, Linkermann A, Jouan-Lanhouet S, Walczak H, Vandenabeele P. Regulated necrosis: the expanding network of non-apoptotic cell death pathways. Nat Rev Mol Cell Biol. 2014; 15:135–147. [PubMed: 24452471]
27. Degterev A, Huang Z, Boyce M, Li Y, Jagtap P, Mizushima N, et al. Chemical inhibitor of nonapoptotic cell death with therapeutic potential for ischemic brain injury. Nat Chem Biol. 2005; 1:112–119. [PubMed: 16408008]
28. Li JX, Feng JM, Wang Y, Li XH, Chen XX, Su Y, et al. The B-Raf(V600E) inhibitor dabrafenib selectively inhibits RIP3 and alleviates acetaminophen-induced liver injury. Cell Death Dis. 2014; 5:e1278. [PubMed: 24901049]

29. Sun L, Wang H, Wang Z, He S, Chen S, Liao D, et al. Mixed lineage kinase domain-like protein mediates necrosis signaling downstream of RIP3 kinase. Cell. 2012; 148:213–227. [PubMed: 22265413]
30. Zhao J, Jitkaew S, Cai Z, Choksi S, Li Q, Luo J, et al. Mixed lineage kinase domain-like is a key receptor interacting protein 3 downstream component of TNF-induced necrosis. Proc Natl Acad Sci USA. 2012; 109:5322–5327. [PubMed: 22421439]
31. McCall K. Genetic control of necrosis – another type of programmed cell death. Curr Opin Cell Biol. 2010; 22:882–888. [PubMed: 20889324]
32. Kim SJ, Li J. Caspase blockade induces RIP3-mediated programmed necrosis in Toll-like receptor-activated microglia. Cell Death Dis. 2013; 4:e716. [PubMed: 23846218]
33. Fortes GB, Alves LS, de Oliveira R, Dutra FF, Rodrigues D, Fernandez PL, et al. Heme induces programmed necrosis on macrophages through autocrine TNF and ROS production. Blood. 2012; 119:2368–2375. [PubMed: 22262768]
34. Bursch W, Ellinger A, Gerner C, Frohwein U, Schulte-Hermann R. Programmed cell death (PCD). Apoptosis, autophagic PCD, or others? Ann N Y Acad Sci. 2000; 926:1–12.
35. Aredia F, Giansanti V, Mazzini G, Savio M, Ortiz L, Jaadane I, et al. Multiple effects of the Na+/H + antiporter inhibitor HMA on cancer cells. Apoptosis. 2013; 18:1586–1598. [PubMed: 23996609]
36. Seglen PO, Gordon PB. 3-Methyladenine: specific inhibitor of autophagic/lysosomal protein degradation in isolated rat hepatocytes. Proc Natl Acad Sci USA. 1982; 79:1889–1892. [PubMed: 6952238]
37. Puertollano R. mTOR and lysosome regulation. F1000Prime Rep. 2014; 6:52. [PubMed: 25184042]
38. Liu Q, Qiu J, Liang M, Golinski J, van Leyen K, Jung JE, et al. Akt and mTOR mediate programmed necrosis in neurons. Cell Death Dis. 2014; 5:e1084. [PubMed: 24577082]
39. Martelotto L, Ng C, Piscuoglio S, Weigelt B, Reis-Filho J. Breast cancer intra-tumor heterogeneity. Breast Cancer Res. 2014; 16:210. [PubMed: 25928070]
40. Polyak K. Heterogeneity in breast cancer. J Clin Invest. 2011; 121:3786–3788. [PubMed: 21965334]
41. Reshkin SJ, Bellizzi A, Caldeira S, Albarani V, Malanchi I, Poignee M, et al. Na+/H+ exchanger-dependent intracellular alkalinization is an early event in malignant transformation and plays an essential role in the development of subsequent transformation-associated phenotypes. FASEB J. 2000; 14:2185–2197. [PubMed: 11053239]
42. Costa CJ, Kirschner LB, Cragoe EJ. Intracellular binding of spin-labeled amiloride: an alternative explanation for amiloride's effects at high concentration. J Cell Physiol. 1987; 130:392–396. [PubMed: 2435744]
43. Yuan TL, Cantley LC. PI3K pathway alterations in cancer: variations on a theme. Oncogene. 2008; 27:5497–5510. [PubMed: 18794884]
44. Davis RJ, Czech MP. Amiloride directly inhibits growth factor receptor tyrosine kinase activity. J Biol Chem. 1985; 260:2543–2551. [PubMed: 2982824]
45. Cho YL, Lee KS, Lee SJ, Namkoong S, Kim YM, Lee H, et al. Amiloride potentiates TRAIL-induced tumor cell apoptosis by intracellular acidification-dependent Akt inactivation. Biochem Biophys Res Commun. 2005; 326:752–758. [PubMed: 15607733]
46. Lin Y, Choksi S, Shen HM, Yang QF, Hur GM, Kim YS, et al. Tumor necrosis factor-induced nonapoptotic cell death requires receptor-interacting protein-mediated cellular reactive oxygen species accumulation. J Biol Chem. 2004; 279:10822–10828. [PubMed: 14701813]
47. Sakon S, Xue X, Takekawa M, Sasazuki T, Okazaki T, Kojima Y, et al. NF-κB inhibits TNF-induced accumulation of ROS that mediate prolonged MAPK activation and necrotic cell death. EMBO J. 2003; 22:3898–3909. [PubMed: 12881424]
48. Shen HM, Lin Y, Choksi S, Tran J, Jin T, Chang L, et al. Essential roles of receptor-interacting protein and TRAF2 in oxidative stress-induced cell death. Mol Cell Biol. 2004; 24:5914–5922. [PubMed: 15199146]
49. Benhar M, Dalyot I, Engelberg D, Levitzki A. Enhanced ROS production in oncogenically transformed cells potentiates c-Jun N-terminal kinase and p38 mitogen-activated protein kinase

activation and sensitization to genotoxic stress. Mol Cell Biol. 2001; 21:6913–6926. [PubMed: 11564875]

50. Zoncu R, Bar-Peled L, Efeyan A, Wang S, Sancak Y, Sabatini DM. mTORC1 senses lysosomal amino acids through an inside-out mechanism that requires the Vacuolar H(+)-ATPase. Science. 2011; 334:678–683. [PubMed: 22053050]
51. Soltoff SP, Mandel LJ. Amiloride directly inhibits the Na,K-ATPase activity of rabbit kidney proximal tubules. Science. 1983; 220:957–958. [PubMed: 6302840]
52. Scaringi L, Cornacchione P, Ayroldi E, Corazzi L, Capodicasa E, Rossi R, et al. Omeprazole induces apoptosis in jurkat cells. Int J Immunopathol Pharmacol. 2004; 17:331–342. [PubMed: 15461867]

Appendix: Supplementary material

Supplementary data to this article can be found online at doi:10.1016/j.canlet.2016.02.042.

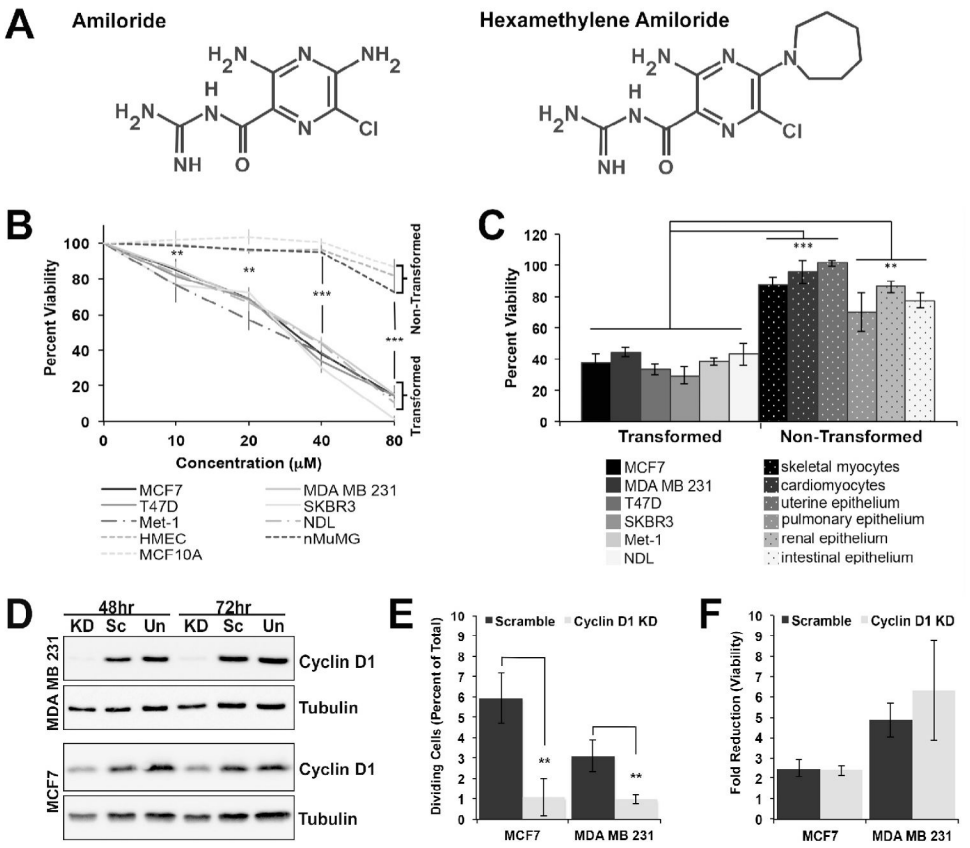

Fig. 1.

HMA specifically depletes breast cancer cells irrespective of their molecular profile or proliferative status. (A) The chemical structures of amiloride and HMA are depicted. (B) The viabilities of human and mouse non-transformed and transformed cell lines treated for 24 hrs with varying concentrations of HMA were assessed by trypan blue exclusion. Data are presented as averages of at least four independent biological trials and expressed as a percent of vehicle control ± SEM. (C) The indicated non-transformed primary cells were exposed for 24 hrs to either vehicle or 40 μM HMA, and their relative viabilities were compared to tumor cell lines from panel B. Data are presented as averages of at least three biological replicates and expressed as a percent of control ± SEM. HMA did not significantly reduce the viability of non-transformed cells ($p > 0.05$ for all tissue types). (D) MDA-MB-231 and MCF7 cells were left untransfected (Un), or were transfected for 48 hrs or 72 hrs with either scrambled (Scr) or cyclin D1 knockdown (KD)-directed siRNA oligonucleotides. Lysates were immunoblotted for cyclin D1 and tubulin loading control. (E) Mitotic MCF7 or MDA-MB-231 cells in anaphase or telophase were determined by morphologic features following DAPI staining after transfection with scrambled or cyclin D1-directed siRNAs. Data are presented as the average mitotic percentage of the total cell population for three replicate experiments ± SEM. (F) Following control or siRNA-mediated cyclin D1 knockdown, cells were exposed to vehicle or 40 μM HMA for 24 hrs, and the total number of viable cells was assessed by trypan blue exclusion. Data are presented as the fold

reduction in cell viability ± SEM as determined from three biological replicates. **$p < 0.01$; ***$p < 0.001$.

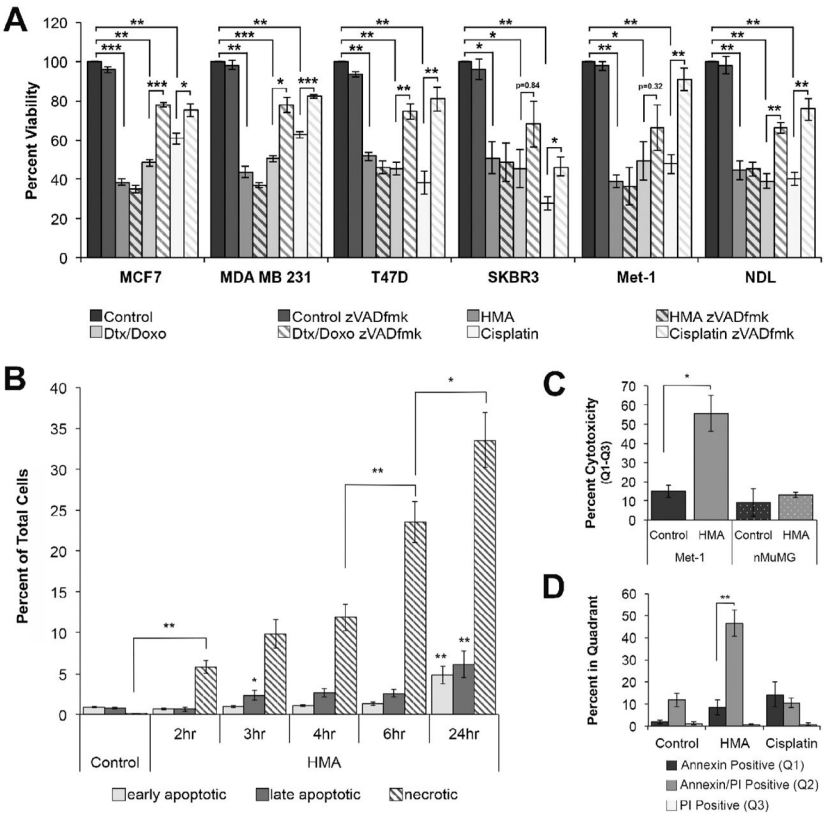

Fig. 2.

HMA induces caspase-independent necrosis in breast cancer cells. (A) MCF7, MDA-MB-231, T47D, SKBR3, Met-1 and NDL cells were pretreated with zVADfmk for 1 hr prior to the administration of vehicle, 40 μM HMA, 40 μM cisplatin or apoptosis inducing agents (170 nM doxorubicin (Doxo) and 50 nM docetaxel (Dtx)) for 24 hrs, and cell viability was determined by trypan blue exclusion assay. Inhibition of caspases failed to attenuate HMA induced cytotoxicity in MCF7 (viability of 38.5 ± 1.5% with HMA alone versus 34.8 ± 2.1% with HMA plus zVADfmk), MDA-MB-231 (43.8 ± 3.2% versus 37.0 ± 2.0%) T47D (51.6 ± 2.2% versus 46.1 ± 6.8%), SKBR3 (50.8 ± 8.0% versus 48.7 ± 5.5%), Met-1 (38.7 ± 3.2% versus 36.6 ± 5.6%) and NDL (44.7 ± 4.9% versus 45.2 ± 3.1%) cells, but rescued cells from death induced by chemotherapeutic agents. Data are presented as averages of three replicate experiments ± SEM. (B) MCF7 breast cancer cells were exposed to 40 μM HMA for varying times, and staining with acridine orange and ethidium bromide was visualized by fluorescence microscopy and quantified. Data are presented as averages of the percent of total cells in early and late apoptosis and in necrosis from three biological replicates (±SEM). Each replicate encompassed counts from a minimum of 2×10^3 cells. (C, D) Met-1 mammary cancer cells and nMuMG non-transformed mammary cells were exposed to vehicle, 40 μM HMA or 50 μM cisplatin for 24 hrs, stained with Annexin-V and propidium iodide, and analyzed by fluorescence activated cell sorting (FACS). Data are presented as ± SEM. *$p < 0.05$; **$p < 0.01$.

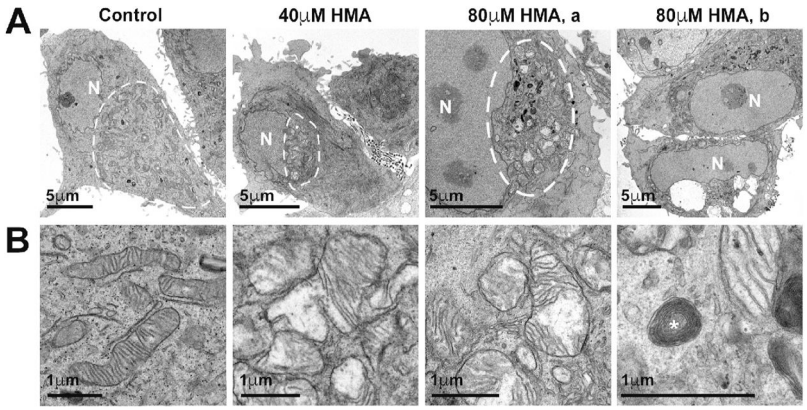

Fig. 3.

HMA induces primary necrosis in breast cancer cells. (A, B) MCF7 breast cancer cells were treated with the indicated concentrations of HMA for 3 hrs and examined by transmission electron microscopy at different magnifications. Organelle distribution relative to the nucleus (N) is encircled in vehicle- and HMA-treated cells and a representative multilamellar structure is indicated with a white asterisk. *$p < 0.05$; **$p < 0.001$.

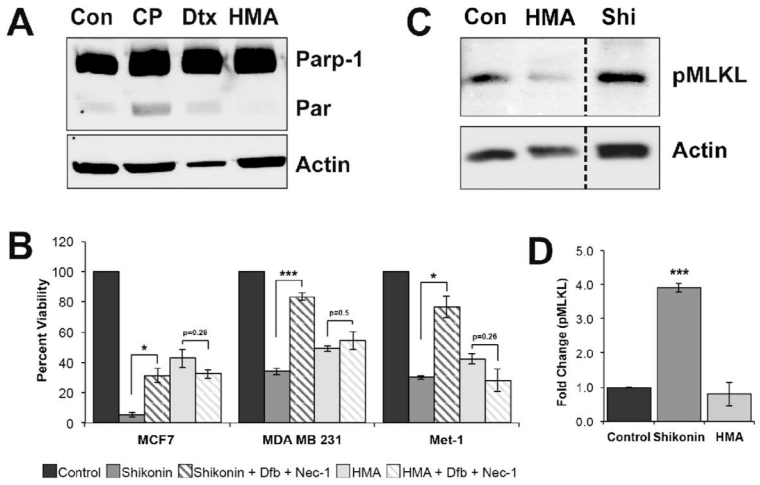

Fig. 4.

HMA does not induce parthanatos or necroptosis. (A) MDA-MB-231 cells were treated for 24 hrs with vehicle control, 40 μM cisplatin (CP), 50 nM docetaxel (Dtx) or 40 μM HMA, and lysates were immunoblotted for Par/Parp-1 and actin loading control. Blots are representative of three replicate experiments. (B) MCF7, MDA-MB-231 and Met-1 cells were incubated for 24 hrs with vehicle, 40 μM HMA or 3 μM shikonin (Shi), in the presence or absence of both 25 μM necrostatin-1 (Nec-1) and 10 μM dabrafenib (Dfb) as indicated, and cell viability was assessed by trypan blue exclusion. Data are presented as averages ± SEM relative to control from at least three replicate experiments. (C) MDA-MB-231 cells were treated for 24 hrs with vehicle control (Con), 40 μM HMA or 3 μM shikonin, and lysates were immunoblotted for T357/S358 phosphorylated MLKL and actin loading control. Blots are representative of three replicate experiments. Dashed line indicates where blot was trimmed to remove extraneous lanes. (D) Quantification of phosphorylated MLKL protein levels for three replicate experiments, expressed as a fold change in phospho-MLKL after normalization to actin loading control. *$p < 0.05$; **$p < 0.01$; ***$p < 0.001$.

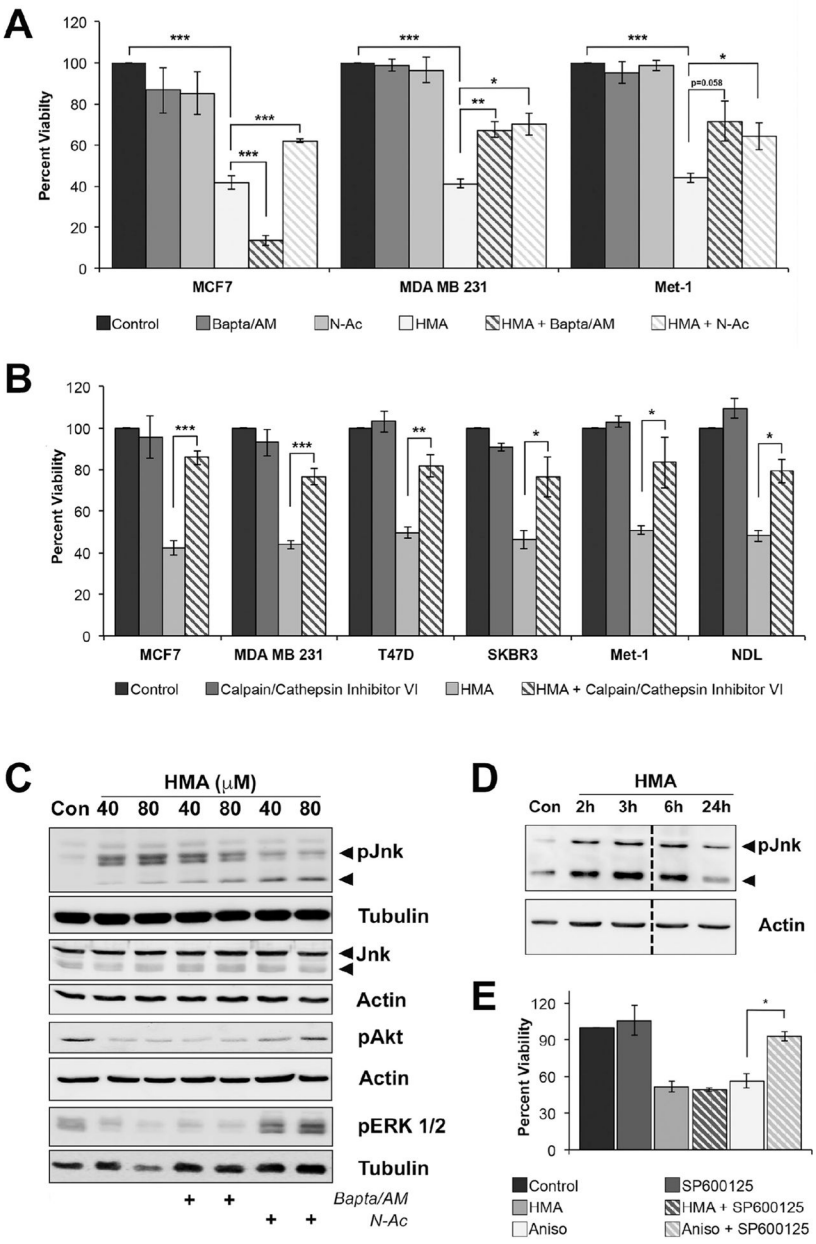

Fig. 5.

HMA-induced cytotoxicity is rescued by the inhibition of ROS and lysosomal proteases. (A) MCF7, MDA-MB-231 and Met-1 cells were pre-incubated for 1 hr with vehicle, 10 μM Bapta/AM or 5 mM N-Ac prior to 24 hr treatment with vehicle or 40 μM HMA, and cell viability was assessed by trypan blue exclusion. (B) MCF7, MDA-MB-231, T47D, SKBR3, Met-1 and NDL cells were pre-incubated for 1 hr with vehicle or 20 nM Calpain Inhibitor VI prior to 24 hr treatment with vehicle or 40 μM HMA, and cell viability was assessed by trypan blue exclusion. (C) MDA-MB-231 cells were pretreated for 1 hr with vehicle, 10 μM Bapta/AM, or 5 mM N-Ac and then treated with vehicle (Con), or 40 μM or 80 μM HMA. Cell lysates were immunoblotted with antibodies to Jnk, phospho-Jnk, phospho-Akt, phospho-Erk1/2 and tubulin loading control. (D) MDA-MB-231 cells were treated for

various times with vehicle (Con) or 40 μM HMA, and lysates were immunoblotted with antibodies to phospho-Jnk or actin loading control. Dashed line indicates where blot was trimmed to remove extraneous lanes. (E) MDA-MB-231 cells were pre-incubated for 1 hr with vehicle or 50 μM SP600125 prior to 24 hr treatment with vehicle, 40 μM HMA or 2.5 μg/mL anisomycin (Aniso), and cell viability was assessed by trypan blue exclusion. *$p < 0.05$; **$p < 0.01$; ***$p < 0.001$.

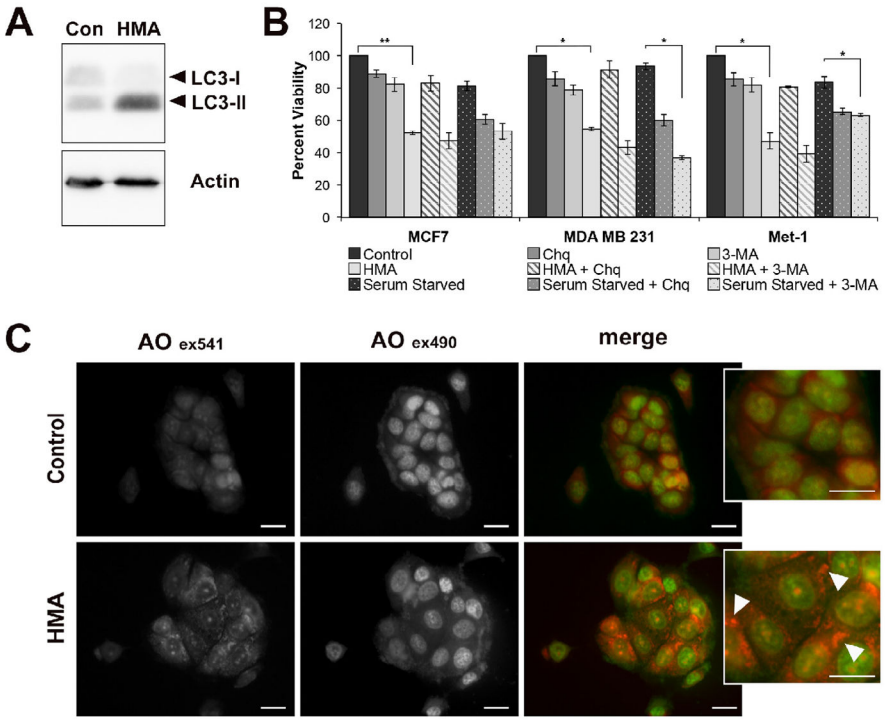

Fig. 6.

HMA acts through lysosomes independent of autophagic processes. (A) MDA-MB-231 cells were treated with 40 μM HMA for 24 hrs, and lysates were immunoblotted for LC3 and actin loading control. (B) MCF7, MDA-MB-231 and Met-1 cells were pretreated for 24 hrs with vehicle, 5 mM 3-MA or 50 μM chloroquine (Chq), followed by treatment with vehicle or HMA, or by serum starvation. 3-methyl adenine pretreatment failed to rescue the viability of HMA-treated cells ($p > 0.05$ for all cell types). Data are presented as averages of three replicate experiments ± SEM and are expressed as a percent of the control. (C) Nucleic acids and acidic vesicles were stained in MCF7 cells with acridine orange after treatment for 3 hrs with vehicle control or 40 μM HMA. A selected region is magnified to show detail, note the aggregation of lysosomes with HMA treatment (arrowhead). Scale bar = 20 μm. *$p < 0.05$; **$p < 0.01$; ***$p < 0.001$.

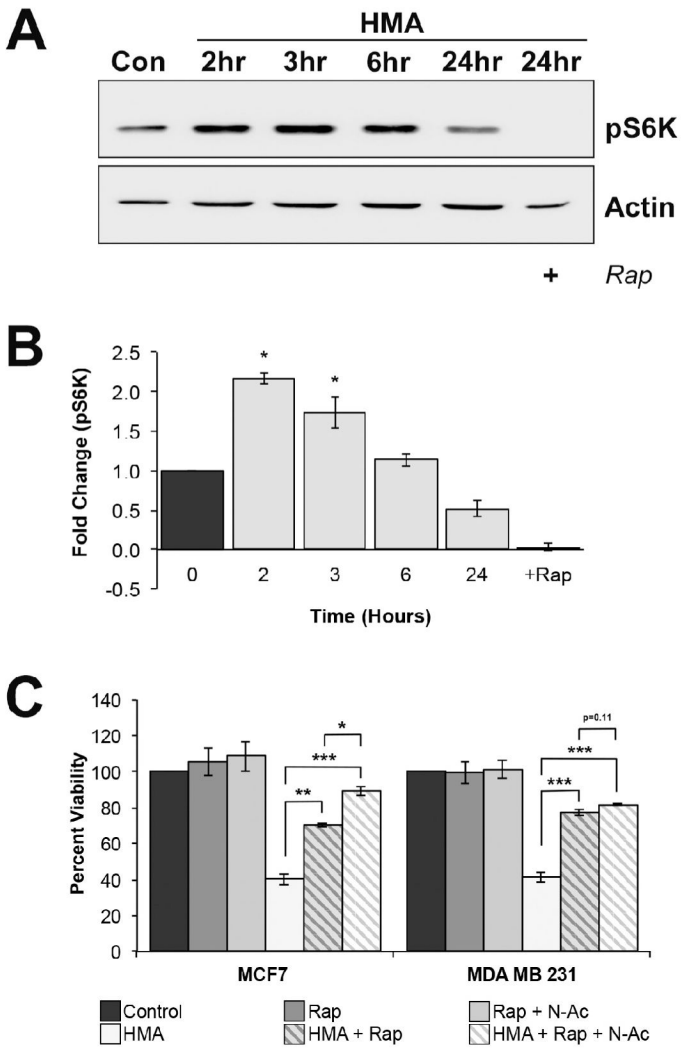

Fig. 7.

HMA-mediated cytotoxicity depends on the activation of mTOR. (A) MDA-MB-231 cells were treated for various times with 40 μM HMA in the presence or absence of 1 μM rapamycin (Rap), and lysates were immunoblotted for phospho-S6 kinase (pS6K) and actin loading control. (B) Replicate blotting experiments such as that illustrated in panel A were quantified. Data are presented as the fold change in pS6K levels relative to vehicle control after normalization to actin. (C) MCF7 and MDA-MB-231 cells were pretreated with vehicle, 1 μM rapamycin or rapamycin plus 5 mM N-Ac, and sensitivity to 24 hr treatment with 40 μM HMA was determined. Data are presented as average percent viability of three replicate experiments relative to vehicle control. *$p < 0.05$; **$p < 0.01$; ***$p < 0.001$.